Geofluids (2002) **2**, 95–107

Transfer of hydrocarbons from natural seeps to the water column and atmosphere

I. R. MACDONALD[1], I. LEIFER[2], R. SASSEN[1], P. STINE[1], R. MITCHELL[3] AND N. GUINASSO JR[1]

[1]Texas A&M University — GERG, College Station, TX, USA; [2]University of California, Chemistry Department, Santa Barbara, CA, USA; [3]Earth Satellite Corp., Rockville, MD, USA

ABSTRACT

Results from surface geochemical prospecting, seismic exploration and satellite remote sensing have documented oil and gas seeps in marine basins around the world. Seeps are a dynamic component of the carbon cycle and can be important indicators for economically significant hydrocarbon deposits. The northern Gulf of Mexico contains hundreds of active seeps that can be studied experimentally with the use of submarines and Remotely Operated Vehicles (ROV). Hydrocarbon flux through surface sediments profoundly alters benthic ecology and seafloor geology at seeps. In water depths of 500–2000 m, rapid gas flux results in shallow, metastable deposits of gas hydrate, which reduce sediment porosity and affect seepage rates. This paper details the processes that occur during the final, brief transition — as oil and gas escape from the seafloor, rise through the water and dissolve, are consumed by microbial processes, or disperse into the atmosphere. The geology of the upper sediment column determines whether discharge is rapid and episodic, as occurs in mud volcanoes, or more gradual and steady, as occurs where the seep orifice is plugged with gas hydrate. In both cases, seep oil and gas appear to rise through the water in close proximity instead of separating. Chemical alteration of the oil is relatively minor during transit through the water column, but once at the sea surface its more volatile components rapidly evaporate. Gas bubbles rapidly dissolve as they rise, although observations suggest that oil coatings on the bubbles inhibit dissolution. At the sea surface, the floating oil forms slicks, detectable by remote sensing, whose origins are laterally within ~1000 m of the seafloor vent. This contradicts the much larger distance predicted if oil drops rise through a 500 m water column at an expected rate of ~0.01 m s^{-1} while subjected to lateral currents of ~0.2 m s^{-1} or greater. It indicates that oil rises with the gas bubbles at speeds of ~0.15 m s^{-1} all the way to the surface.

Key-words: bubble model, gas hydrate, hydrocarbon seep, oil slick, remote sensing

Received 6 August 2001; accepted 29 November 2001

Corresponding author: Ian R. MacDonald, Texas A&M University — GERG, College Station, TX 77843, USA.
E-mail: ian@gerg-tamu.edu. Tel: +979 862 2323. Fax: +979 862 1347.

Geofluids (2001) **2**, 95–107

INTRODUCTION

Hydrocarbon migration through shallow marine sediment is a widespread phenomenon on the continental margins throughout the world (Kvenvolden 1993). Over geological time, the hydrocarbon seep process returns large amounts of carbon from thermogenic sources to the biosphere (Macgregor 1993), but the rates and magnitudes of this process are very poorly understood. Kvenvolden & Harbaugh (1983) have given a 'best' estimate for global input of 2.5×10^8 L $year^{-1}$ of oil entering the world oceans from natural seepage. However, this estimate was based on relatively few data from real-world seeps. Satellite remote sensing imagery readily detects layers of floating oil that form over active seeps (Espedal & Wahl 1999), providing a means to estimate the rates at which seeps are flowing (MacDonald *et al.* 1993) and to survey the numbers of hydrocarbon seeps across oil-producing regions (Kornacki *et al.* 1994; MacDonald *et al.* 1996). Recent studies that utilized comprehensive collections of remote sensing imagery have provided evidence that seepage in the Gulf of Mexico contributes oil at a rate of $(0.4–1.1) \times 10^8$ L $year^{-1}$ (Mitchell *et al.* 1999). Because this is such a large fraction of the global total estimated by Kvenvolden & Harbaugh (1983), it is probable that their estimate should be revised upwards. A better understanding of seep geology and geochemistry will improve the accuracy of new estimates of global and regional seep rates. In particular, factors that cause seepage rates to vary over time need to be examined.

Seeps form where migration is rapid and ongoing. Organic enrichment from the oil and gas produces profound alteration of surface sediments, including the precipitation of carbonates and colonization by dense aggregations of

chemosynthetic fauna (MacDonald *et al.* 1989). The formation and dissociation of gas hydrate deposits are important components of hydrocarbon seeps because very large quantities of methane can accumulate in geologically recent sediments. The Gulf of Mexico is one of several continental margins where gas hydrate deposits occur in the uppermost portion of the sediment column (Brooks *et al.* 1984). Many shallow deposits of gas hydrate are located there in water depths of 500–2000 m (Milkov *et al.* 2000). The gas hydrates in the Gulf of Mexico often form as a mélange of oil and sediments and are an important substratum for microbial and metazoan life forms (MacDonald *et al.* 1994; Sassen *et al.* 1998). Loop-current eddies and other circulation events episodically warm the bottom waters covering the hydrate. Direct observations indicate that gas venting through shallow gas hydrate deposits exhibits fluctuations that correspond closely to variations in bottom water temperature (MacDonald *et al.* 1994; Roberts *et al.* 1999). More extreme fluctuations in discharge have been observed from seeps associated with mud volcanoes (MacDonald *et al.* 2000; Roberts & Carney 1997).

The prevalence of hydrocarbon seeps in the Gulf of Mexico provides a natural laboratory for studying the effects of seepage. Many of the sites are well mapped and include hydrocarbon plumes that vent from predictable locations. Overall, however, attempts to measure the hydrocarbon flux remain simplistic and time dependent. Basic information regarding the size distribution of gas bubbles, the ratio of gas to oil in seep plumes, the rise speed of drops and bubbles and the velocity of bubble-induced upwelling flow has only been described in preliminary form. An important goal of studying seeps is to understand the fate of seeping hydrocarbons: what fraction dissolves into the water column, disperses into the atmosphere or oxidizes through biological processes. In this paper, we provide details on the aspects of seep geology and dynamics of the seep process that affect the temporal variability in the amount of oil and gas released, the geochemistry of the constituents and their fate in the ocean.

STUDY AREA

The northern Gulf of Mexico contains over 200 active seeps, as determined by satellite remote sensing surveys (Earth Satellite Corporation 1997; Mitchell *et al.* 1999). Approximately 80% of these are concentrated in the region south of Louisiana and Texas (Fig. 1). Oils in this region are predominantly

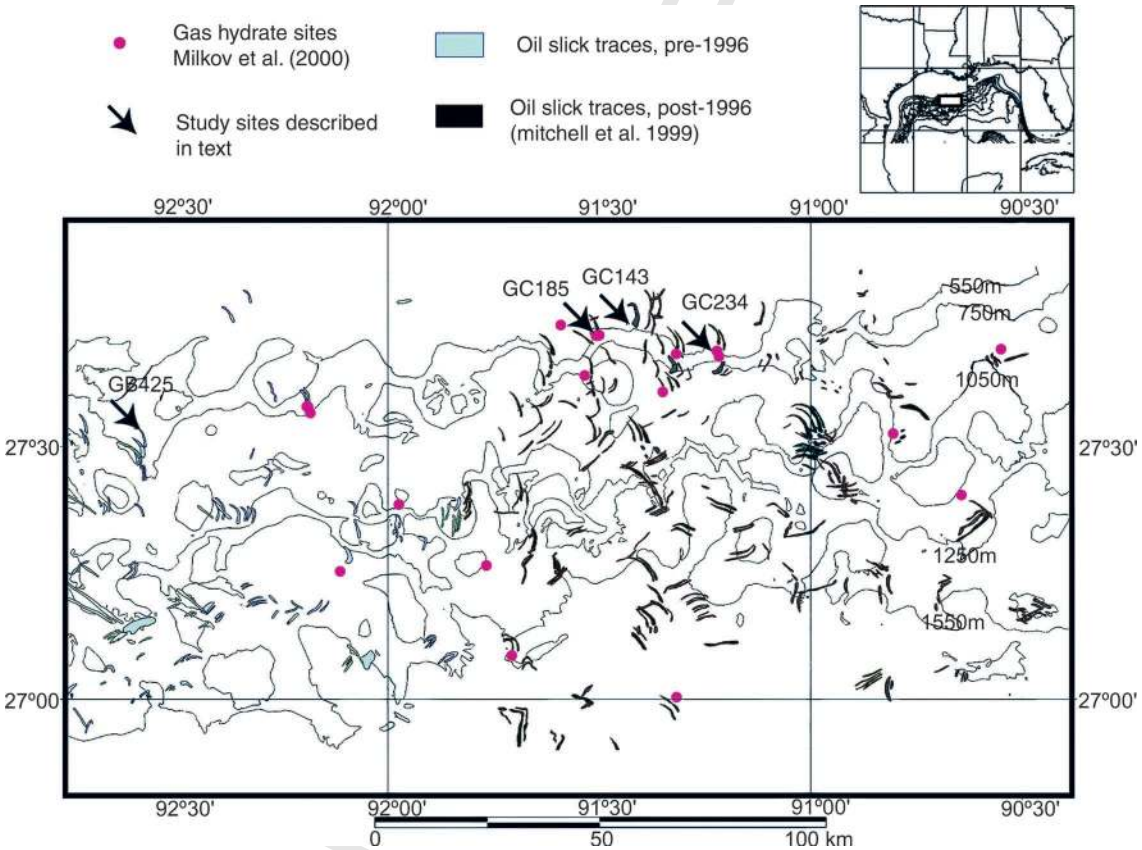

Fig. 1. Locations of floating oil from natural origins (slicks) imaged by satellite remote sensing in the northern Gulf of Mexico (Earth Satellite Corporation 1997). Inset map shows location relative to the southern USA. Recent slick outlines were imaged primarily in 1996 and 1997; historic slick outlines are taken from archival images that predate this survey. Shallow gas hydrates were collected with 6 m piston cores in various surveys (Milkov *et al*. 2000).

medium-weight crude from an upper Jurassic source rock. They migrate upward into unconsolidated strata through faults generated by active and extensive salt tectonics (Sassen *et al.* 1993). The exploration of these seeps and associated chemosynthetic communities with the use of submarines dates to 1986 (MacDonald *et al.* 1989). However, most of the work has been done in water depths of less than 1000 m because most of the available submarines are limited to that depth. A fundamental distinction among seeps is whether the locality includes active fluid discharge, as can be the case in mud volcanoes, or is plugged by shallow deposits of gas hydrate (MacDonald 1998). We present examples from sites representative of seepage processes in the Gulf of Mexico. Two examples are sites where gas hydrates occur at the seabed and two are mud volcanoes where fluids are actively discharging.

The main seep discussed here is a hydrate site designated GC185 (the lease block number), which was the first hydrocarbon seep community to be sampled from a submersible (MacDonald *et al.* 1989). The seep area is a mound extending about 300 m from east to west and 500 m from north to south. The mound, which is composed of mud, carbonate and shallow gas hydrate, has a crest depth of 570 m and rises about 40 m above the surrounding seafloor (MacDonald *et al.* 1994). Surface sediments contain, by weight, as much as 10% liquid hydrocarbons (Kennicutt *et al.* 1988). A perennial plume of fine bubbles and small drops of oil escapes from the top of the mound. A second site, GC234, is located at a similar depth some 20 km to the west. Here, numerous smaller mounds of shallow gas hydrate interrupt the seafloor across a slope formed by a half-graben. The hydrate-dwelling polychaete, *Hesiocaeca methanicola*, was described from specimens collected at this site (Fisher *et al.* 2000).

The deeper of the mud volcano sites is designated GB425. It is located on the western edge of the Auger Basin, an intraslope basin that contains economically significant amounts of hydrocarbons in the Auger, Cardamom and Macaroni fields. A steep-sided and flat-topped mound that extends approximately 0.7 km × 1.0 km at a summit depth of 570 m is located midway along the seep-affected region of the Auger Basin. Active fluid expulsion has created a 50 m wide, subcircular mud lake on the south-western edge of the summit. Methane escapes from a point at the centre of the mud lake in a steady stream, punctuated by episodic pulses of oil expelled when the volcano erupts (MacDonald *et al.* 2000). A second mud volcano site is designated GC143. This is a very active feature in a water depth of 320 m (Neurauter & Roberts 1994). At this site, oil and gas are emitted in an intermittent stream through a large mud lake.

MATERIALS AND METHODS

Remote sensing detection of floating oil utilized a variety of available satellite data, including synthetic aperture radar (SAR) from the European Radar Satellite (ERS) and Canadian Radarsat platforms, as well as Landsat Thematic Mapper images. Radar or light energy received from layers of oil floating on the ocean has a low backscatter coefficient and appears 'dark' compared to backscatter from adjacent 'bright' ocean areas. Natural oil layers, also called *slicks*, are distinguished from biogenic surfactant layers by having fewer broad and parallel bands, which have distinct termini and describe acute angle curves as floating oil drifts with the wind and current (Espedal & Wahl 1999; MacDonald *et al.* 1993). Wind speeds in surface areas covered by satellite images were in the range 2–7 $m\,s^{-1}$, based on estimates provided by commercial weather services. Areas of floating oil were quantified by thresholding data to the intensity range of identified slicks and supervising the resulting classification to eliminate possible weather phenomena. The outlines of the slicks were manually digitized and compiled in a geographical information system database (ArcView).

Seafloor sampling and observation were conducted with the submarine Johnson Sea Link (JSL). This is a battery-operated vehicle that carries two scientists and two operators. The JSL was fitted with a variety of sampling devices. Sediment samples were collected with push cores, which are short lengths of butyrate tubing mounted on a tee-handle and pushed into the seafloor by the mechanical arm of the JSL. Samples of gas hydrate were collected with a modified push core that featured a sharpened metal coring tube. The tube was used to chip pieces of gas hydrate loose from exposed deposits. The loosened pieces then floated up into the top tube. When collection was complete, the tube was placed in an insulated pressure chamber that was then sealed to preserve bottom water temperature and pressure. In practice, the chamber was recovered with internal temperatures of 8 °C, which approximates ambient bottom water temperatures. Internal pressure, however, was in the range 2–3 MPa, which is less than the ~5.4 MPa hydrostatic pressure present at 540 m depth. This pressure and temperature were adequate to keep the gas hydrate samples intact until they could be preserved in liquid nitrogen. To sample the fluids associated with gas hydrate, small pieces were allowed to fully decompose in loosely closed vials held at room temperature.

Geophysical survey data often provide useful overviews of possible hydrocarbon reservoirs and migration conduits that might produce natural hydrocarbon emissions. However, because there are many relic seeps in the Gulf of Mexico, identifying active seeps requires confirmation by direct observation and sampling. Streams of oil and gas rising from the seafloor were generally imaged in the output from precision depth recorders. Surveillance aircraft were sometimes used to locate active seeps and would do so by searching for slicks. Once a slick had been located, the ship would follow it upwind to where oil drops could be seen surfacing. Although surfacing drops temporally spread into small circles of rainbow sheen, continued spreading rapidly thins the floating oil into an all but invisible layer.

Samples of floating oil slicks were collected from small boats deployed from the research vessel during periods of relatively calm weather. To sample a slick, 25 cm × 25 cm pieces of 0.05 mm nylon mesh were attached to a shallow-sided frame whose bottom was a coarse metal screen. The frame was positioned laterally under the portion of water containing the slick. The frame was then lifted straight up through the layer so that the water drained through the screen. This operation was repeated 10 times and the nylon mesh was removed into a clean glass jar. The frame and screen were thoroughly rinsed with solvent between samples. To collect a time-series of oil after it had surfaced, a small, flat float was placed in the water near the surfacing position. The small boat could then follow along as the float drifted with the oil, moving in periodically to retrieve a sample. The time-series presented here was collected during calm sea conditions and mid-summer temperatures.

Laboratory analysis of whole-oil samples was conducted with gas chromatography using a flame ionization detector (GC-FID). The analytical methods have been described in detail by Kennicutt *et al.* (1987). The chromatographs presented in this paper were optically scanned from the original ink traces and then digitally re-touched in PhotoShop to remove calibration markings and to standardize the axes.

A bubble model was applied to simulate the processes occurring during the rise of methane bubbles for seepage conditions at GC185 in the Gulf of Mexico. Bubbles simulated spanned a range of radii from 0.1 to 1 cm. Because contamination with surfactants greatly affects the transfer rate of gases, simulations of 'clean' and 'dirty' bubbles were considered. The bubble model is described in detail in Leifer & Patro (in press). In essence, the model solves the complete, coupled differential equations describing the size, depth and molar and pressure changes for each gaseous component. Bubble break-up was not simulated, although bubbles larger than 7 mm were observed to be unstable and rapidly broke up. Parameterizations of rise velocity and bubble gas transfer rate for each gas are based on best available literature sources. Unfortunately, published oily bubble parameterizations are largely unavailable, and contaminated bubble parameterizations were used. Thus the bubble gas loss flux is probably an upper limit because the oil coating, which is thicker than a surfactant layer, is most likely to reduce gas outflow further.

Three cases were simulated and are summarized in Table 1. Also shown in Table 1 are the equilibrium partial pressures (H) for the dissolved gas as calculated by Henry's law constant. Environmental values were constant throughout the water column, a reasonable first assumption in the absence of observations of conditions inside the bubble stream except for the first few metres above the seabed. For all simulations, air (oxygen and nitrogen) was in equilibrium with atmospheric values, the water temperature was 5 °C and the water depth and bubble release depth were 540 m. In Case 1, the upwelling flow velocity (V_{up}), observed at the seabed, of

Table 1 Parameterization of three cases simulated in the bubble dissolution model. H is Henry's law constant and V_{up} is the upwelling flow velocity. For all simulations, air (oxygen and nitrogen) was in equilibrium with atmospheric values, the water temperature was 5 °C and the water depth was 540 m.

Case	V_{up} (cm s^{-1})	H [CH_4] (atm)	[CH_4] (μmol cm^{-3})
1	10	0.01	1.73×10^{-2}
2	0	0.01	1.73×10^{-2}
3	0	0.25	4.33×10^{2}

~10 cm s^{-1} was assumed to extend throughout the water column, and the dissolved CH_4 concentration was equivalent to 0.01 atm (low case). In comparison with the bubble CH_4 pressure, this is a negligible level. If the bubbles significantly disperse or dissolve, V_{up} throughout much of the water column may be significantly less. Case 2 had no upwelling flow and the same dissolved CH_4 concentration. Dissolved CH_4 may be significantly enhanced in the bubble plume and Case 3 simulated a much higher dissolved CH_4 concentration equivalent to 0.25 atm.

The trajectory of oil drops rising from the seafloor was predicted using a simulation program (SLIKTRAK), which has been described by Venkataramaiah (1996). This model predicts the three-dimensional migration path of hydrocarbon drops from the seafloor to the surface. When oil drops arrive in the surface layer, SLIKTRAK calculates the drift path of the resulting slick. The migration path calculations are based on a random walk algorithm parameterized with forced driving (current, wind or buoyancy) and random driving (dispersion) factors for each layer in the water column. Model output consists of the positions of particles (oil drops) at specified time-steps. For this simulation, the water column was treated as a uniform layer, i.e. there was no variation in current direction or speed with depth. The random walk offsets were simulated as independent, normal (0, 1) excursions scaled to 1% of the velocities in the x, y and z directions. Particle rise speed can be specified independently for each water column layer, but for the present work rise speeds were simulated as constant. Currents were derived from a 24 h time-series recorded at 10 min intervals at 50 m depth at a platform near the GC185 location. Surface drift was derived from hourly wind records for this area and time.

RESULTS

Distribution and characteristics of oil slicks

The regional distribution of oil slicks detected by satellite remote sensing is shown in Fig. 1. The survey comprised imagery from two distinct time periods (Earth Satellite Corporation 1997). Historic data were archived images mostly collected prior to 1993. Recent data were images collected during 1996 and 1997. In most cases, weather records were consulted to verify that wind speeds for the images were

compliant with slick formation. The ocean area contained in an individual image depends upon the type of satellite platform. Overall, the survey provides a comparison of the activity of individual seeps over time. The results confirm earlier observations suggesting that some seeps appear to be more or less perennial (Kornacki *et al.* 1994; MacDonald *et al.* 1996); in other words, they produce a visible slick in the same general location in multiple images. Other seeps form prominent slicks in one or more satellite images, but not in others. This suggests an episodic or intermittent seep process similar to that observed at mud volcanoes (MacDonald *et al.* 2000). Location overlays of shallow gas hydrates have been collected (Milkov *et al.* 2000) and indicate that nine of the locations where oil slicks were visible in multiple images correspond to gas hydrate sites (Fig. 1). These locations include the GC185 and GC234 sites. Fewer data are available concerning the distribution of mud volcanoes, but two mud volcanoes, GC143 and GB425, have been visited and sampled with submarines. An oil slick was detected in the historic data set near the GC143 site, but not in the more recent data. Slicks were not detected at GC425 in the recent data, and the slick present in the historic data appears to have originated from a position several kilometres to the south in much deeper water. The GB425 volcano is known to have erupted vigorously in 1997 with a significant release of oil (MacDonald *et al.* 2000).

Another feature evident in remote sensing data is the distinctive shapes of oil slicks (Espedal & Wahl 1999; MacDonald *et al.* 1993). The leading end of the slicks, called the *surfacing footprint* herein, is relatively broad and tapers to a fine point along a curving track of 10–15 km. Strikingly, slicks in individual images tend to form in multiple parallel lines; generally, the lines are separated by no more than a few hundred metres. The surfacing footprint of slicks captured in separate images tends to be offset by ~1 km and has tails that drift in different directions, but a perennial seep will produce slick origins within a consistent area, which we designate the *surfacing perimeter*. An examination of the rising stream of bubbles and of photographs of slicks shows some of the causes of these consistent patterns (Fig. 2).

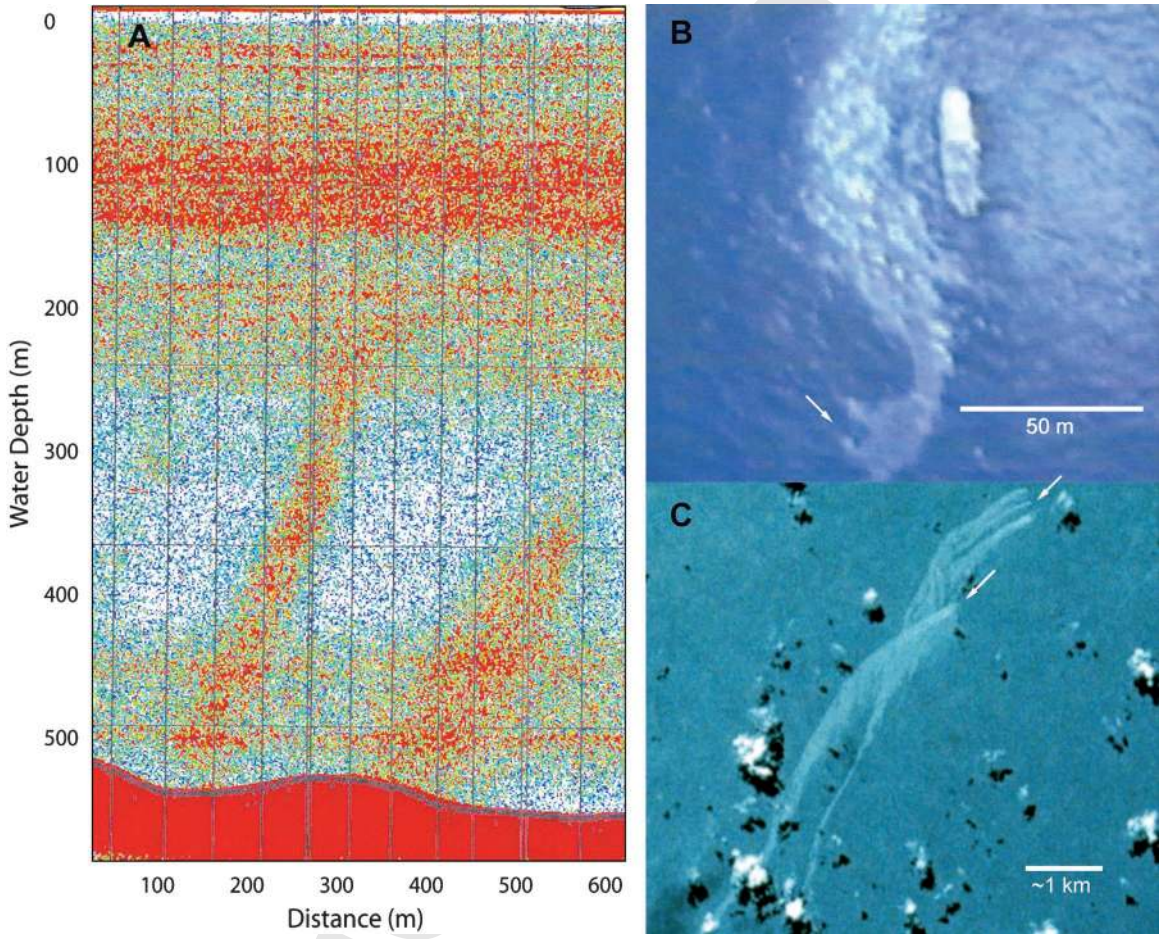

Fig. 2. Formation of natural oil slicks. (A) West to east trace of 25 kHz echo-sounder shows streams of oil and gas rising from two separate vents on the seafloor. Dense returns in mid-water depths of 80–120 m mark the approximate depth of the thermocline. (B) Oil drops reach the surface in a discrete footprint (arrow) and drift past research vessel. Sun-glint is enhanced in area of floating oil. (C) Photograph from the Space Shuttle shows sun-glint from slicks. There appear to be four distinct origins (arrows), probably indicating individual vents on the seafloor.

The acoustic trace of an oil seep was recorded over GC185. Two distinct plumes, separated by a distance of about 300 m, were detected (Fig. 2A). It should be noted that the plumes are deflected from their seafloor origins and become indistinct at a height of 200–300 m above the seafloor. Seafloor observations at GC185 showed that vents associated with shallow deposits of gas hydrate produce streams of bubbles, oil drops and oil-coated bubbles (Fig. 2A). Oil drops were observed spreading on the surface over GC185 as the trace was collected, but aerial overflight imagery was not available.

Aerial photography from another collection cruise shows the origins of an oil slick (Fig. 2B). Here, surfacing oil and bubbles form a slick that drifts past the research vessel. Satellite photography (Fig. 2C) shows multiple, parallel slicks drifting and co-mingling. These observations suggest a model in which oil rises in a stream that maintains a relatively narrow cross-section all the way to the surface. Thus, distinct seafloor vents would produce distinct surfacing footprints. In transit to the surface, currents within the water column deflect the stream, as can be clearly seen in the angled rise path of the plumes in Fig. 2(A). The factors that could influence deflection distance are the rise speed of the oil, the magnitude and direction of the currents and the height of the water column. If these factors have a characteristic range at individual seeps, the streams would reach the surface within a predictable surfacing perimeter.

Effects in the seabed

The relationship between the persistence of seepage and seafloor geology depends on the degree to which sediments, gas hydrate deposits or fluidized mud will retard the escape of hydrocarbons. A qualitative assessment of this is evident in photographs of gas venting from a hydrate deposit (Fig. 3A) or the mud-filled crater of a mud volcano (Fig. 3B). Gas hydrate deposits, particularly those that breach the seafloor, exist at equilibrium between hydrate formation in the gas-saturated pore volume of the shallow sub-bottom and hydrate dissociation at the water–hydrate interface. The deposits breach and vent where gas flux is most vigorous. Exposed hydrate produces a steady stream of fine bubbles. Sediments in the Gulf of Mexico seeps can contain as much as 10% by weight of liquid hydrocarbons (Kennicutt *et al.* 1987). Gas hydrate deposits often trap oil in underlying pools (MacDonald *et al.* 1994) or incorporate oil within the hydrate matrix (Sassen *et al.* 2001). As the hydrate dissociates, the oil incorporated in the hydrate matrix is released and mixes with escaping gas. Gas release from hydrate deposits is probably temperature dependent, as rising bottom water temperatures reduce hydrate stability (MacDonald *et al.* 1994; Roberts *et al.* 1999), and may be punctuated when large chunks of the material break free from the bottom and float towards the surface (Suess *et al.* 1999). A very different situation exists in mud volcanoes where the viscous mud, generally suspended in a hypersaline brine, forms a dense fluid lining the vents where gas and oil escapes. This material offers scant resistance to buoyant gas and oil and frequently releases very large bubbles (Fig. 3B).

Alteration of seeping oil

Residence time in the near-surface sediments is reflected in the chemical signature of seep oil. At mud volcanoes, hydrocarbons migrate rapidly through the sediment column with little geochemical alteration. Where surface deposits of gas hydrate are present, hydrocarbon discharge is impeded, at least temporarily, and geochemical alteration of the trapped material transpires over a longer time. Microbial degradation of near-surface oil greatly depletes the normal and branched alkanes in the oil and produces an end product comprising an unresolved complex mixture of tars (Kennicutt *et al.* 1988). Samples of seep oils show different degrees of degradation (Fig. 4). From the rapid migration regime at the GC143 mud volcano, we collected seep oil over the vent with a submarine. In this sample, alkanes and cyclic compounds showed little alteration (Fig. 4A). In contrast, a highly degraded oil extracted from sediments adjacent to a hydrate deposit at GC185 produced a sample in which the alkanes, isoprenoids and aromatics had been entirely degraded (Fig. 4B). Oil extracted from recovered pieces of gas hydrate at GC185 showed extensive degradation, but was intermediate between sediment oil and oil from the mud volcano (Fig. 4C). This indicates that occlusion in a hydrate matrix may preserve oil from microbial effects to some degree. Oil rising to the sea surface would have distinct chemical signatures depending on whether it originated from a hydrate deposit or a mud volcano. Accurate interpretation of this information depends on whether the chemical composition is further altered in transit.

Alteration of seep oil floating on the sea surface is graphically portrayed by a 1 h time-series showing the concentrations of normal alkanes in samples of floating oil taken in the surfacing footprint of a slick formed over a mud volcano (Fig. 5). The change in alkane ratio for floating oil is dramatic and rapid. Within 12 min of surfacing, the modal peak in normal alkane concentrations shifted from C_{17} to C_{23}, with a corresponding loss of lighter alkanes. This ratio remained essentially unchanged through the remainder of the time-series, although concentrations apparently decreased. This effect is probably due to evaporation, with dissolution playing a small role (Fingas 1995). The total distance covered during the time-series was about 750 m, indicating a drift speed for the floating slick of about 2 m s^{-1}.

Modelling bubble dissolution

Another mechanism for the alteration of hydrocarbons that escape from seeps is dissolution of gas in the water column

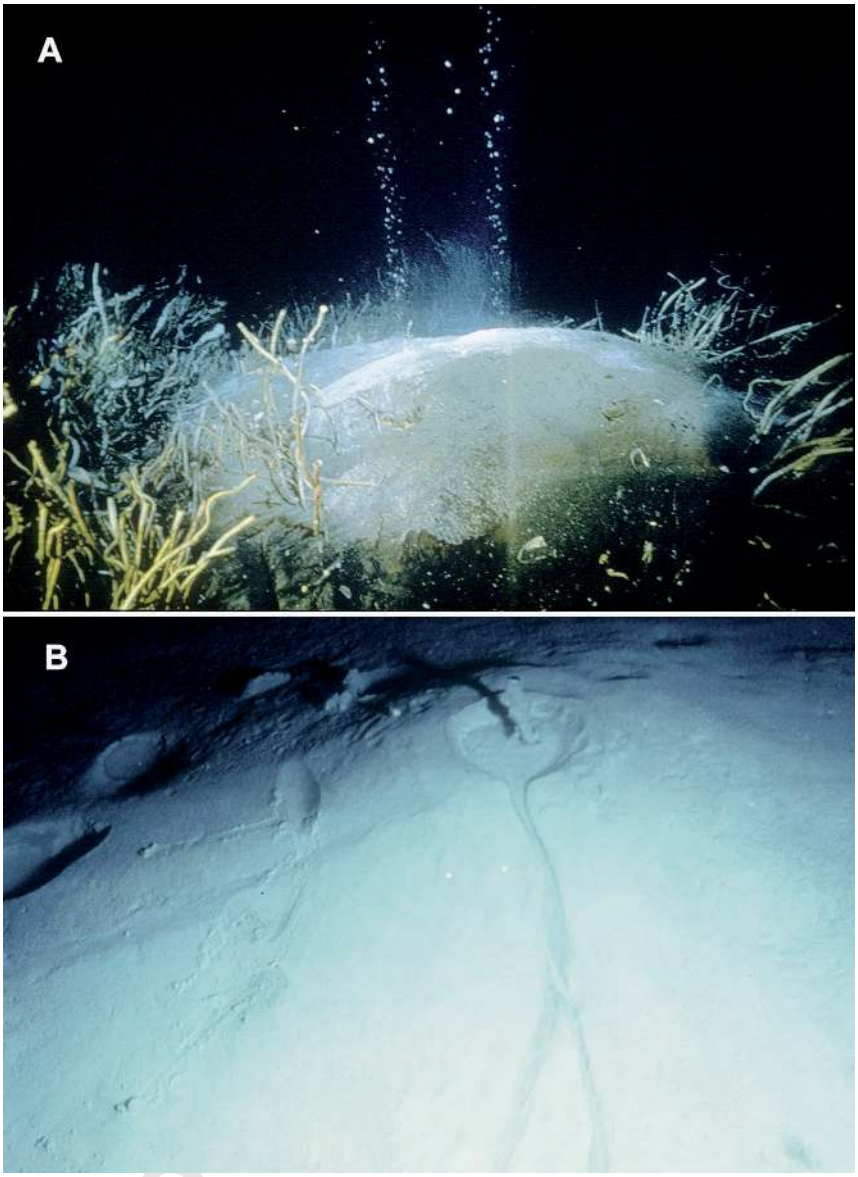

Fig. 3. Styles of gas venting at natural seeps in the Gulf of Mexico. (A) Bubbles of gas, which are often contaminated with oily coatings, escape from a shallow deposit of gas hydrate at 570 m water depth; the exposed portion of the mound is about 1 m across (photograph by Ian R. MacDonald). (B) Single large bubble of gas rises from a pool of brine on a small mud volcano; diameter of crater is about 25 cm (photograph by Jane Thrasher).

during transit to the surface. Although we have no direct data on dissolved methane concentrations in the water column above the seep, it is possible to constrain the properties of the oil and gas stream by modelling the response of the oil and gas to physical and chemical processes in the water column. A bubble model was applied to simulate the rise of pure methane bubbles spanning a range of radii (r) of 0.1–10 mm under seepage conditions at GC185.

There are several factors that affect the depth at which a bubble dissolves. The initial size of the bubbles is determined by the shape and size of the orifice where the bubble forms (Blanchard & Syzdek 1977). Bubble size is important because the rate at which bubbles transfer gas to the surrounding ocean is highly size dependent, and because the quantity of gas a bubble can lose increases cubically with size. Contamination of bubbles with surfactants or oil greatly reduces the rate at which gas can dissolve through the bubble–water interface. The bubble-induced upwelling flow and elevated dissolved CH_4 concentrations in the bubble stream can strongly affect bubble survival. The rising mass of bubbles causes upward fluid movement that allows a stream of bubbles to reach the surface in less time than an individual bubble would require to rise the same distance. Upwelling flows were observed at GC185 a few metres above the seabed. Bubble dissolution into the fluid can increase ambient CH_4 concentration and raise the dissolution gradient. A bubble in a stream of other bubbles would therefore transfer gas to the water column more slowly than an individual bubble. The

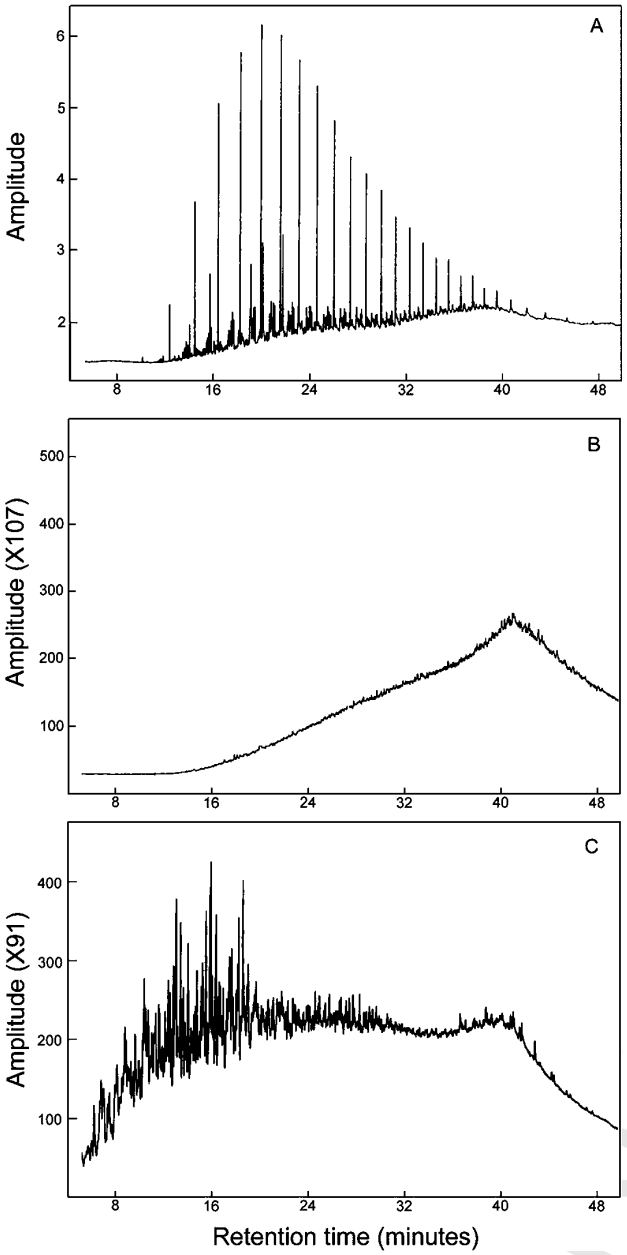

Fig. 4. Chromatographs of seep oil collected by submarines and analysed by gas chromatography with flame ionization detection. (A) Rapidly venting oil collected from active mud volcano at GC143. (B) Oil extracted from sediments adjacent to gas hydrate deposit in GC185. (C) Oil extracted from gas hydrate sample collected in GC185.

bubble model simulated dissolution of CH_4 from contaminated (oily) and noncontaminated bubbles rising through a 540 m water column under three sets of conditions (Table 1).

For contaminated bubbles, the ratio of final to initial r at the surface is shown in Fig. 6(A), while, for bubbles that dissolved subsurface, the dissolution depth is shown in Fig. 6(B). For upwelling flow and low dissolved CH_4 (Case 1), only bubbles larger than 3 mm survive to the surface. Bubbles of ~4 mm reached the surface without changing size (i.e. growth from decreasing hydrostatic pressure and air inflow equalled shrinkage due to CH_4 loss). Bubbles larger than 5 mm more than doubled in size by the time they surfaced; thus, they probably would have broken into smaller bubbles during their ascent.

Two bubble vents were observed at GC185, one in which pulses of bubbles were emitted, and which produced a broad distribution of bubble size, and one in which bubble size was sharply peaked. The grey shaded area in Fig. 6 indicates the sharply peaked distribution size of bubbles. With an upwelling flow (Case 1), most of the bubbles in this size range dissolved between 175 and 350 m depth. In the absence of an upwelling flow (Case 2), these bubbles dissolved even more deeply, although there was a larger size dependence.

Enhancement of dissolved methane (Case 3) has an even larger effect than the upwelling flow (compare Cases 2 and 1), with bubbles larger than 3 mm reaching the surface. This enhancement is minimal for the smallest bubbles that dissolve in the first 100 m, as the pressure difference between the bubble and the fluid is still extremely large. For the largest bubbles though, the loss of methane is not as great. When the dissolved methane in the water in the bubble stream is nontrace (i.e. CH_4 dissolution into the water is greater than diffusion out of the bubble stream), bubble dissolution is slower, and bubbles arrive at the surface larger. For the largest bubbles ($r > 7$ mm), the effect of the decreased rise time due to the upwelling flow is more important than the decreased outflow rate, particularly because over most of the lifetime of these bubbles the dissolved CH_4 concentration is negligible relative to the bubble internal pressure (which drives the outflow).

In all cases, most of the bubbles ($r < 3.5$–4 mm) dissolved during their rise; thus, only the largest had the potential to reach the surface. However, bubbles larger than ~6 mm reached the surface having doubled in size (i.e. r at the surface was >1 cm), and mostly would have broken up into smaller bubbles that dissolved. Thus, only a very narrow size range of the observed bubbles had the potential to reach the surface. One assumption is that the bubbles are contaminated (dirty) throughout their rise, and thus that oil plays an important role in enhancing bubble survivability. The three cases in Table 1 were simulated again, but this time with clean bubbles, and the results are shown in Fig. 6(C,D). Clean bubbles represent an upper limit that may be appropriate for large bubbles. Observations of the rise velocity of nonoily, contaminated, bubbles in seawater show that the hydrodynamic behaviour of bubbles larger than 1000 μm is similar to that of clean bubbles (Patro *et al.* 2001; Tsuchiya *et al.* 1997). As the simulations show, only 1 cm radius bubbles potentially can reach the surface, and these bubbles would have broken into smaller bubbles in the first few metres. Most of the bubbles dissolved in the first 100 m.

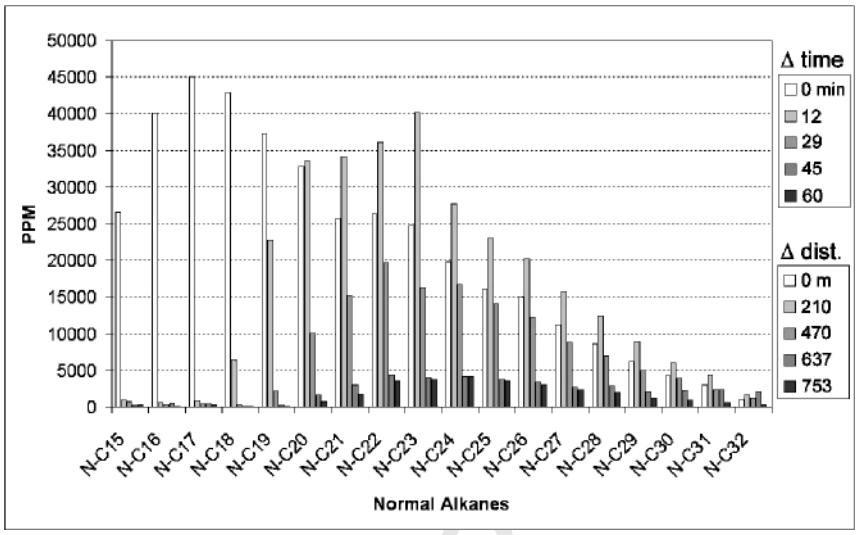

Fig. 5. Histograms show successive changes in ratio of normal alkanes for oil drifting on the sea above a seep. Samples of oil were collected immediately after surfacing and at ~15 min intervals as the oil drifted with wind and current.

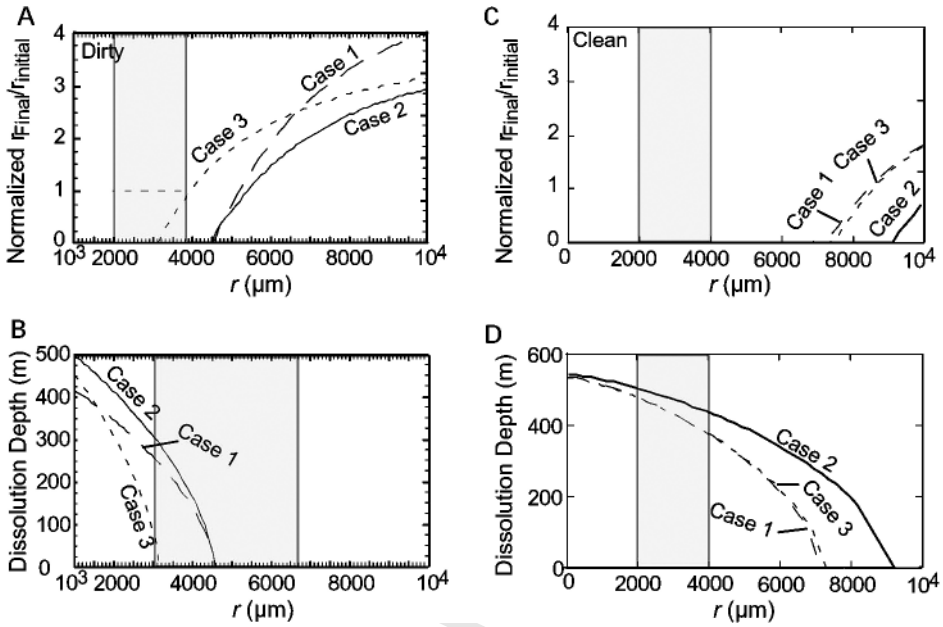

Fig. 6. Model simulations of bubble size change and dissolution rates. (A) Normalized ratio of final to initial bubble radius at the surface for different initial bubble radius, *r*, for dirty bubbles. (B) Bubble dissolution depth for dirty bubbles. (C) Normalized ratio of final to initial bubble radius at the surface for different initial bubble radius, *r*, for clean bubbles. (D) Bubble dissolution depth for clean bubbles. Conditions for each case are described in the text.

Modelling slick formation

To examine the interaction of seeps and water column processes in the formation of oil slicks and to determine what reasonable range of circumstances produce slicks similar to those observed in remote sensing imagery, the rise of oil and gas from the bottom to the surface was simulated. Three cases were simulated, with rise rates for the fluid particles of 40, 15 and 1 cm s^{-1}. These rates are, respectively, the mean and maximum speeds for seep bubbles observed at the seep sites (Leifer & MacDonald submitted) and the velocity for a 1 cm diameter sphere with the density of a medium-weight crude oil as calculated from Stoke's law. Each simulation treated particle ensembles released at hourly intervals during a 24 h period. The currents were adapted from acoustic Doppler current profile records recorded at a deep-water platform in the northern Gulf of Mexico; the profile interval was 4.5 m and the time-step was 5 min (Bela James 2000,

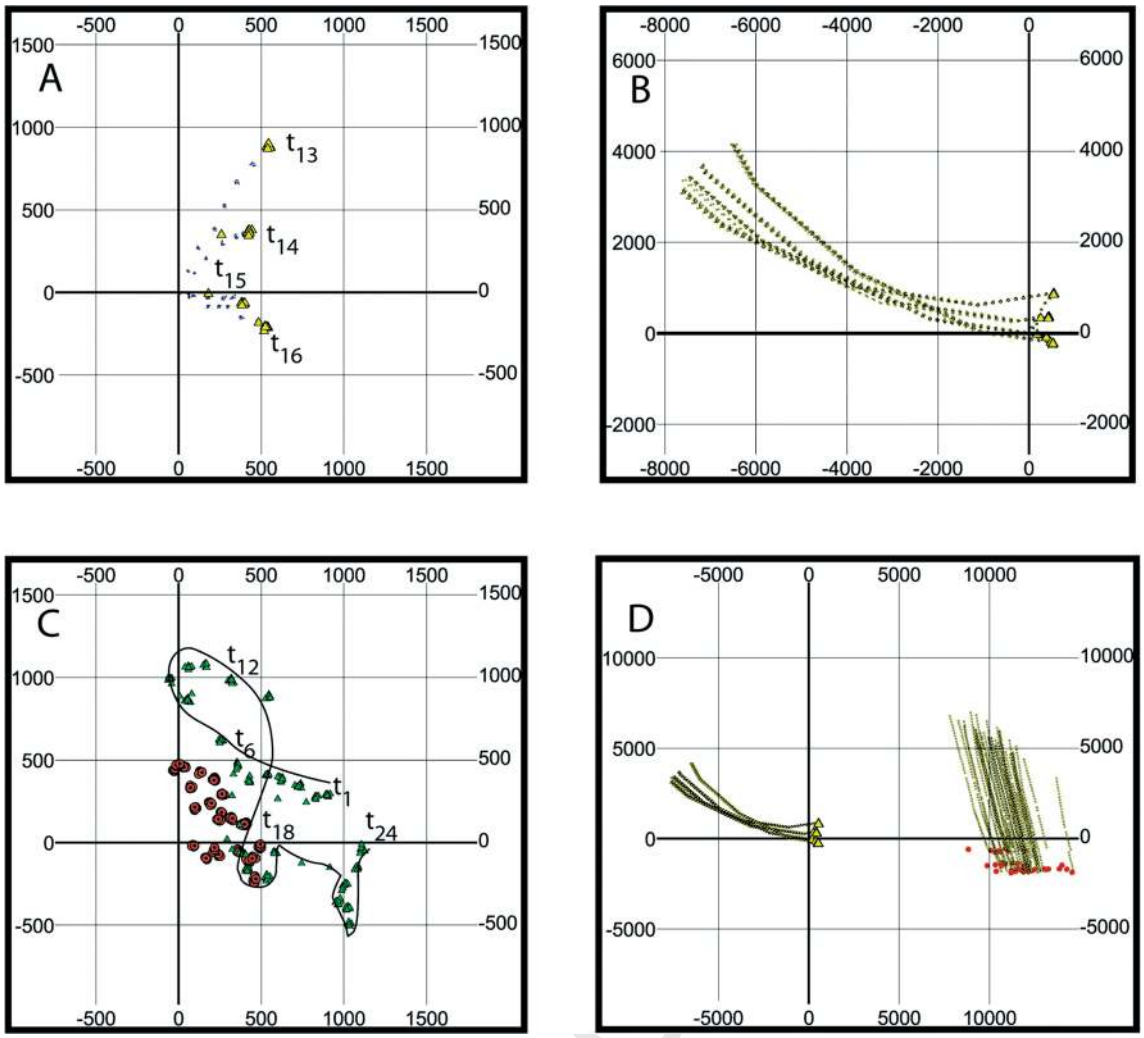

Fig. 7. Simulated rise and drift trajectories for hourly ensembles of particles with different rise speeds. Simulation applies a 24 h time-series of magnitude and direction for current profiles and wind. Water depth is 570 m. Scales are in metres relative to release point. (A) Rise path (dots) and surfacing footprints (triangles) for four ensembles of particles rising at 15 cm s^{-1}. Surfacing times are at hours 13–16 of the simulation. (B) Drift path for particles shown in previous example. (C) Progression of surfacing footprints for particles rising at 15 cm s^{-1} (triangles) and 40 cm s^{-1} (circles). Line shows approximate progression path of slower particles during the 24 h simulation. (D) Comparison of surfacing footprint and drift path for particles rising at 15 cm s^{-1} (triangles) and 1 cm s^{-1} (small circles). Both sets of particles were released at the same time and were subjected to the same current and wind conditions.

personal communication). The wind time-series was adapted from a gridded product archived at Texas A&M University; the time-step was 3 h (Matt Howard 2000, personal communication). Wind and current time-series were identical for each simulated case.

The results of these simulations are summarized in Fig. 7. The direction and distance of deflection from the origin depended upon current profiles during the rise period. Figure 7(A) shows four hourly ensembles released at hourly time-steps t_{13}, t_{14}, t_{15} and t_{16}, midway during the 24 h simulation interval. The plot shows the rise path of the ensembles and their surfacing footprints. At t_{13}, the rise path is deflected to the north-east and the surfacing footprint is offset from the source by ~1000 m. As the current direction and magnitude changed during the subsequent 3 h, the direction of deflection shifted to the east and south-east and the offset was reduced to about 500 m. Figure 7(B) shows the drift path of the floating particles as they moved with wind and surface currents for about 12 h after surfacing. It should be noted that the drift paths reproduce the curvilinear trajectory and length of actual slicks observed in remote sensing imagery (Fig. 2C). Interestingly, the time-step between the releases of particle ensembles also reproduced the braided appearance of multiple individual slicks, which is also evident in the remote sensing imagery. Earlier, we noted that discrete vents on the seafloor could produce the distinctive series of parallel slicks observed in imagery data. This result shows that pulsed releases over a short time period would produce a similar pattern.

Figure 7(C,D) compares the effects of different rise speeds. In Fig. 7(C), the surfacing footprints for hourly ensembles of the 15 cm s^{-1} case and the 40 cm s^{-1} case are plotted for the entire 24 h simulation. Both cases produced looping trajectories of points as the surfacing footprints were deflected in different directions by changing currents. The slower rise speed produces a larger surfacing perimeter than the faster rise speed because a longer residence in the water column results in greater particle deflection by currents. Particles rising at 15 cm s^{-1} reached the surface within an elliptical surfacing perimeter that had a long axis aligned north-west to south-east over a distance of ~1500 m and a short axis of about 600 m. Particles that rose at 40 cm s^{-1} reached the surface within a similarly shaped ellipse whose long axis was ~800 m. In Fig. 7(D), the surfacing footprints and drift path of the simulation shown in Fig. 7(B) are compared with a similar subset of particles that were set to rise at 1 cm s^{-1}, the calculated rise speed of centimetre-sized oil drops.

DISCUSSION

The remote sensing survey compiled by Earth Satellite International (Earth Satellite Corporation 1997; Mitchell *et al.* 1999) documents the prevalence of natural seepage across the entire northern Gulf of Mexico; a portion of this area is shown in Fig. 1. These data confirm comprehensively some of the characteristics of hydrocarbon seepage that had been previously reported. Seeps are fixed geological features over annual or multiannual timescales. Therefore visible effects of individual seeps will be localized. Oil escaping from a seep can create a perennial slick on the sea surface above its seabed location (Kornacki *et al.* 1994; MacDonald *et al.* 1996). The slicks have distinctive shapes that can help to distinguish natural oil seeps from pollution or other phenomena (Espedal & Wahl 1999; MacDonald *et al.* 1993).

Other trends in the remote sensing data are less distinct, but do indicate important directions for research. Shallow deposits of gas hydrates co-occur with many seeps (MacDonald *et al.* 1994; Sassen *et al.* 2001); nine of the hydrate sites plotted in Fig. 1 are associated with surface slicks. Seafloor observations confirm that the material that contributes to the formation of surface slicks in many cases emanates from gas hydrate deposits, e.g. Fig. 2(B). However, additional geological surveys are required to determine a predictive relationship between surface slicks and gas hydrate deposits, because surface slicks have been found intermittently associated with mud volcanoes, where gas hydrate deposits are not indicated (MacDonald *et al.* 2000). Because the Earth Satellite International remote sensing imagery was collected over different time periods (separated by years in many cases), the survey gives some information regarding the constancy or intermittency of seepage. There are examples of perennial and intermittent slicks in the remote sensing data, but continual surveillance of individual seeps would be required to define the timescales for seepage. Available evidence is adequate to theorize that gas hydrate deposits produce relatively steady discharge and mud volcanoes produce more punctuated flow.

Bubble dissolution is important in determining where methane from the seeps enters the water column and is an important transport mechanism for oil. Due to their much lower density, bubbles rise significantly more rapidly than oil droplets, and thus the potential for oil droplet dispersion is much less if oil is primarily transported to the sea surface on the bubble surfaces rather than as individual oil droplets. This clearly demonstrates the effect of contamination of these large bubbles, and, in particular, oil contamination. Sonar images of bubbles just 100 m below the surface strongly support the important role of oil in bubble survivability and conversely the role of bubbles in vertically transporting oil, reducing its dispersion and allowing the formation of oil slicks (e.g. Fig. 2A).

Modelling of slick formation was carried out using a greatly simplified (uniform) current profile and distinctly different rise speeds for bubbles and drops. Under these conditions, the pattern produced by the slower particles is radically different from that of particles rising at the approximate speed of bubbles. Slow particles require over 20 h to reach the surface. During this time, water column currents carry the particles more than 10 km from the source. Random motion during the rise path adds much more scatter to the surfacing footprint; the result is that particle ensembles no longer cluster at the scale seen in remote sensing images (Fig. 2B,C). Because slow particles begin their surface drift paths from a much more dispersed distribution, the collective trajectories no longer follow distinct traces. Under simplified conditions, therefore, oil drops will not produce perennial slicks.

Time-course samples along a drifting slick show that the floating oil is rapidly altered on the surface. Laboratory experiments with water washing over a range of temperatures (20–80 °C) have shown that the main effect is in fractions lighter than C_{15} (Larfarge & Barker 1988). The present results were therefore most strongly driven by evaporation that occurred as the surfacing oil underwent the initial spreading into a thin layer. The odour of petroleum was distinct in the vicinity of the surfacing footprint and the evaporation process was undoubtedly enhanced by warm summer conditions. The implication is that the more toxic aromatics released by the oil would tend to be concentrated in the immediate vicinity of the surfacing footprint and would be more likely to affect the atmosphere than the ocean. The change in the overall floating volume is a semiquantitative result due to the imprecise methods used for sampling the slick. Nevertheless, the decrease indicates that the floating layer contains progressively less oil as it drifts away from the source. The final sample was taken <1 km from the source and contained barely detectable traces of oil. It is remarkable, in the light of this loss rate, that slicks remain visible in the remote sensing images over lengths of ~10 km or more

(Fig. 2C). Evidently, very small quantities of floating oil will still produce the remote sensing signature.

The complex variability of slick shape and direction is clearly a result of changing wind and current in the surface layer. The size of apparent surfacing perimeters over active seeps suggests that the oil rises at speeds in the range 10–50 $cm\,s^{-1}$. The model fails to produce slick-like signatures when particle rise speeds approximate those of a bubble-free oil drop. This argues strongly for the interaction of oil and gas during a significant part of the rise path. Oil drops rising without gas would take much longer to reach the surface if the water column was highly stratified, and might be transported significant distances from the source. An example of probable mid-water transport of oil has been reported from the southern Caribbean by Harvey *et al.* (1979), who sampled crude oil from a subsurface layer that evidently originated from a source several hundred kilometres away. Our principal interpretation of these results is that oil slicks that consistently form in the vicinity of a seep are the result of bubble-mediated transport of oil to the surface. Additional real-world measurements are needed to test this conclusion. The Gulf of Mexico is a fruitful setting for sampling and experimentation that can quantify the fluxes of hydrocarbons from natural seeps.

ACKNOWLEDGEMENTS

We thank the captain and crew of the RV Seward Johnson and the Johnson Sea Link submersible for their unstinting assistance. Comments from A. Judd and an anonymous reviewer were extremely helpful during the revision of this paper. Programmatic support from the National Undersea Research Foundation, University of North Carolina Center and the Minerals Management Service, Gulf of Mexico OCS Regional Office is gratefully acknowledged. Exxon Mobil supported development of the SLIKTRAK model.

REFERENCES

Blanchard DC, Syzdek LD (1977) Production of air bubbles of a specified size. *Chemical Engineering Science*, **32**, 1109–12.

Brooks JM, Kennicutt MC II, Fay RR, McDonald TJ, Sassen R (1984) Thermogenic gas hydrates in the Gulf of Mexico. *Science*, **223**, 696–8.

Earth Satellite Corporation (1997) *Gulf of Mexico Marine Oil Seep Survey.* Earth Satellite Corporation, Rockville, MD.

Espedal H, Wahl T (1999) Satellite SAR oil spill detection using wind history information. *International Journal of Remote Sensing*, **20**, 49–65.

Fingas M (1995) A literature review of the physics and predictive modelling of oil spill evaporation. *Journal of Hazardous Materials*, **42**, 157–75.

Fisher CR, MacDonald IR, Sassen R, Young CM, Macko SA, Hourdez S, Carney RS, Joye S, McMullin E (2000) Methane ice worms: *Hesiocaeca methanicola* colonizing fossil fuel reserves. *Naturwissenschaften*, **87**, 184–7.

Harvey GR, Requejo AG, McGillivary PA, Tokar JM (1979) Observation of a subsurface oil-rich layer in the open ocean. *Science*, **205**, 999–1001.

Kennicutt MC, Brooks JM, Denoux GJ (1988) Leakage of deep, reservoired petroleum to the near surface on the Gulf of Mexico continental slope. *Marine Chemistry*, **24**, 39–59.

Kennicutt MC, Sericano J, Wade T, Alcazar F, Brooks JM (1987) High-molecular weight hydrocarbons in the Gulf of Mexico continental slope sediment. *Deep-Sea Research*, **34**, 403–24.

Kornacki AS, Kendrick JW, Berry JL (1994) The impact of oil and gas vents and slicks on petroleum exploration in the deepwater Gulf of Mexico. *Geo-Marine Letters*, **14**, 160–9.

Kvenvolden KA (1993) Gas hydrates — geological perspective and global change. *Reviews of Geophysics*, **31**, 173–87.

Kvenvolden KA, Harbaugh JW (1983) Reassessment of the rates at which oil from natural sources enters the marine environment. *Marine Environmental Research*, **10**, 223–43.

Larfarge E, Barker C (1988) Effect of water washing on crude oil compositions. *American Association of Petroleum Geologists Bulletin*, **72**, 263–76.

Leifer I, MacDonald IR (Submitted) Dynamics of the gas flux from shallow gas hydrate deposits: interaction between oily hydrate bubbles and the oceanic environment. *Earth and Planetory Science Letters.*

Leifer IS, Petro RK (in press) The bubble mechanism for transport of methane from the shallow sea bed to the surface: A review and sensitivity study. *Continental Shelf Research*, in press.

MacDonald IR (1998) Habitat formation at Gulf of Mexico hydrocarbon seeps. *Cahiers de Biologie Marine*, **39**, 337–40.

MacDonald IR, Boland GS, Baker JS, Brooks JM, Kennicutt IIMC, Bidigare RR (1989) Gulf of Mexico chemosynthetic communities II: spatial distribution of seep organisms and hydrocarbons at Bush Hill. *Marine Biology*, **101**, 235–47.

MacDonald IR, Buthman D, Sager WW, Peccini MB, Guinasso NL Jr (2000) Pulsed oil discharge from a mud volcano. *Geology*, **28**, 907–10.

MacDonald IR, Guinasso NL Jr, Ackleson SG, Amos JF, Duckworth R, Sassen R, Brooks JM (1993) Natural oil slicks in the Gulf of Mexico visible from space. *Journal of Geophysical Research*, **98**, 16 351–64.

MacDonald IR, Guinasso NL Jr, Brooks JM, Sassen R, Lee S, Scott KT (1994) Gas hydrates that breach the sea-floor and interact with the water column on the continental slope of the Gulf of Mexico. *Geology*, **22**, 699–702.

MacDonald IR, Reilly JF Jr, Best SE, Venkataramaiah R, Sassen R, Amos J, Guinasso NL Jr (1996) A remote-sensing inventory of active oil seeps and chemosynthetic communities in the northern Gulf of Mexico. In: *Hydrocarbon Migration and its Near-Surface Expression, AAPG Memoir*, **66** (eds Schumacher D, Abrams MA), pp. 27–37. American Association of Petroleum Geologists, Tulsa, OK.

Macgregor D (1993) Relationships between seepage, tectonics and subsurface petroleum reserves. *Marine and Petroleum Geology*, **10**, 606–19.

Milkov AV, Sassen R, Norikova I, Mikhailov E (2000) Gas hydrates at minimum stability water depths in the Gulf of Mexico: significance to geohazard assessment. *Gulf Coast Association of Geological Societies Transactions*, **L**, 217–24.

Mitchell R, MacDonald IR, Kvenvolden KK (1999) Estimates of total hydrocarbon seepage in to the Gulf of Mexico based on satellite remote sensing images. In: *Ocean Sciences Meeting*, **OS41I-02**. American Geophysical Union, San Antonio, TX.

Neurauter TW, Roberts HH (1994) Three generations of mud volcanoes on the Louisiana continental slope. *Geo-Marine Letters*, **14**, 120–5.

Patro R, Leifer I, Bowyer P (2001) Better bubble process modeling: improved bubble hydrodynamics parameterization. In: *Gas Transfer and Water Surfaces, Monograph*, 127 (eds Donelan M, Drennan W, Salzman ES). AGU, Washington, DC.

Roberts HH, Carney RS (1997) Evidence of episodic fluid, gas, and sediment venting on the northern Gulf of Mexico continental slope. *Economic Geology and the Bulletin of the Society of Economic Geologists*, **92**, 863–79.

Roberts H, Wiseman W, Jr, Hooper J, Humphrey G (1999) Surficial gas hydrates of the Louisiana continental slope — initial results of direct observations and in situ data collection. In: *Offshore Technology Conference*, **10770**, pp. 259–272. Offshore Technology Conference, Houston, TX.

Sassen R, Brooks JM, MacDonald IR, Kennicutt IIMC, Guinasso NL Jr, Requejo AG (1993) Association of oil seeps and chemosynthetic communities with oil discoveries, upper continental slope, Gulf of Mexico. *Trans. Gulf Coast Association of Geological Societies*, **43**, 349–55.

Sassen R, MacDonald IR, Guinasso NL, Jr, Joye S, Requejo AG, Sweet ST, Alcala-Herrera J, DeFritas DA, Schink DR (1998) Bacterial methane oxidation in sea-floor gas hydrate: significance to life in extreme environments. *Geology*, **26**, 851–4.

Sassen R, Sweet ST, DeFreitas DA, Morelos JA, Milkov AV (2001) Gas hydrate and crude oil from the Mississippi Fan Foldbelt, downdip Gulf of Mexico salt basin: significance to petroleum system. *Marine Geology*, **32**, 999–1008.

Suess E, Torres ME, Bohrmann G, Collier RW, Greinert J, Linke P, Rehder G, Trehu A, Wallmann K, Winckler G, Zuleger E (1999) Gas hydrate destabilization: enhanced dewatering, benthic material turnover and large methane plumes at the Cascadia convergent margin. *Earth and Planetary Science Letters*, **170**, 1–15.

Tsuchiya K, Mikasa H, Saito T (1997) Absorption dynamics of CO_2 bubbles in a pressurized liquid flowing downward and its simulation in seawater. *Chemical Engineering Science*, **52**, 4119–26.

Venkataramaiah RH (1996) Application of an integrated enviornmental monitoring model for natural hydrocarbon seeps in the Gulf of Mexico. PhD thesis. Texas A&M University, College Station, TX.